Ionothermal Approach to Homo- and Heteroleptic Alkylation of Tellurido Mercurate Clusters for Assembly in Lamellar Crystal Structures

Mirko Tallu, Bertram Peters, Alexander Friedrich, and Stefanie Dehnen*

ABSTRACT: The selective methylation and butylation of chalcogenido metalate clusters by utilizing imidazolium-based ionic liquids turned out to be not only a comparably mild but at the same time also the only known method for postsynthetic alkylation of such species in order to increase their solubility. For additional impact on the crystal structures, selective alkylation with longer alkyl chains was addressed by utilizing the ionic liquid $(C_{10}C_1Im)[BF_4]$ (C_{10} = decyl group at position 1 and C_1 = methyl group at position 3 of the cation's Im = imidazolium ring) for ionothermal syntheses of functionalized tellurido mercurate clusters. Herein, we report three novel compounds, two of which comprise cluster anions that exhibit a selective organic functionalization of their terminal telluride ligands upon in situ alkylation with the ionic liquid: $[Hg_6Te_6(Te_2)_2(TeDec)_2]^{6-}$ (in **1**; Dec = decyl) represents the first decylated chalcogenido metalate cluster. A unique heteroleptic functionalization, combining methylation and decylation, was achieved for the second cluster, $[Hg_6Te_6(Te_2)_2(TeDec)(TeMe)]^{6-}$ (in **2**; Me = methyl). The third cluster is purely inorganic, but based on the same cluster core architecture: $[Hg_4Te_2(Te_2)_2(Te_3)_2]^{4-}$ (in **3**) comprises a tritelluride unit instead of two HgTeR groups (R = Me, Dec). As a consequence of the long alkyl chains, both at the cluster and at the charge-compensating cations, all three crystal structures are characterized by lamellar assemblies of cations and anions. For further comparison of the properties of the organometallic versus purely inorganic compounds, vibrational and optical properties of crystalline samples of the compounds comprising clusters **1** and **3** were studied by means of infrared, Raman, and UV−visible spectroscopy. The results clearly show the effect of the presence of an organic decoration (in **1**) relative to its absence (in **3**), reflected by a red shift of the band gap energy (**1** → **3**) and a replacement of the Te−C bands (in **1**) with bands for tritelluride units (in **3**).

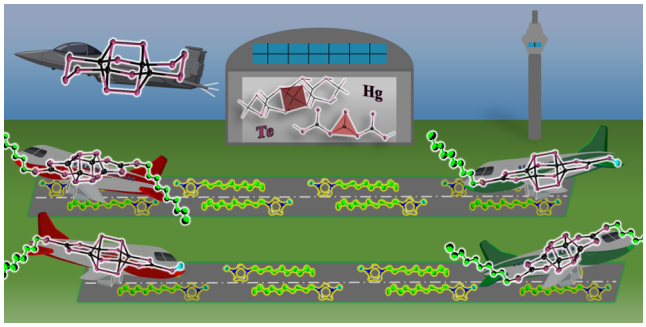

1. INTRODUCTION

The synthesis of crystalline chalcogenido metalate compounds of the type $(Cat)_x[M_yCh_z]$ (Cat = cations, M = metal atoms, Ch = chalcogen atoms) by using long-alkyl-chain amine- or ammonium-based reaction media can afford crystalline compounds exhibiting a notable segregation of cations and anions. If the chain length is large enough, the crystal structures of such compounds can even exhibit a (meso)-lamellar arrangement. In these compounds, the cationic components of the amine-based reaction medium assemble in a polar layer, while the long alkyl chains tend to assemble in nonpolar layers in between, like in soap/surfactant micelles or in lipid double layers known from, e.g., cell membranes.[1] Chalcogenido metalate anions that are integrated in such compounds are embedded in the polar part of the lamellar assembly, and the interlayer spacing depends on the chain length of the reaction medium used. The first examples of such structures were observed in $[C_{12}H_{25}NH_3]_4[Sn_2S_6]\cdot 2H_2O$[2] and $[C_nH_{2n+1}N(CH_3)_{3-m}H_m]_4[Ge_4Ch_{10}]$ (Ch = S, Se; n = 10, 12, 14, 16, 18, m = 0, 1).[3−5] A more recent example comprised a CN-decorated tellurido rhenate cluster that crystallized as $[C_{14}H_{29}N(CH_3)_3]_4[Re_6Te_8(CN)_6]$ in a lamellar arrangement upon surfactant-templated synthesis.[6] A tellurido mercurate cluster with porphyrin-like macrocyclic topology embedded in a lamellar crystal structure, $(C_{10}C_1Im)_8[Hg_8Te_8(Te_2)_4]$ (**A**), was obtained from an ionothermal treatment of $Na_2[HgTe_2]$ with the imidazolium-based ionic liquid $(C_{10}C_1Im)[BF_4]$ comprising long alkyl chains (C_{10} = decyl group at position 1 and C_1 = methyl group at position 3 of the cation's Im = imidazolium ring).[7]

Scheme 1. Illustration of the Syntheses of Compounds 1−3 by Ionothermal Treatment of $Na_2[HgTe_2]$ and $Na_2[Hg_3Te_4]$ in $(C_{10}C_1Im)[BF_4]$ at 80 °C[a]

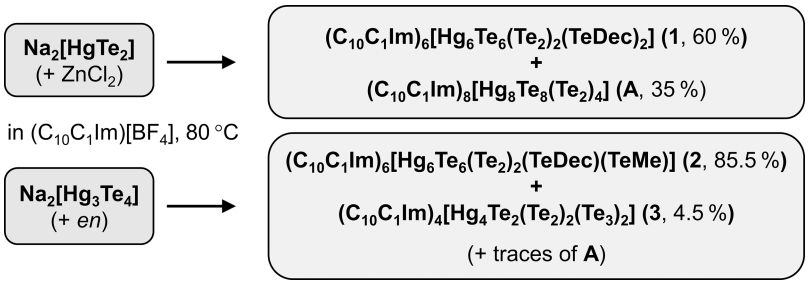

[a]More details are given in the text; en = ethane-1,2-diamine.

Another property of imidazolium-based ionic liquids of the general type $(C_m(C_n)C_oIm)X$ (m, n, o = number of C atoms in the alkyl chains at positions 1, 2, and 3 of the Im ring, X = anion), which was discovered only recently, is their simultaneous function as the reaction medium and reactant during the synthesis of crystalline chalcogenido metalate clusters with organic decoration.[8−13] In this case, the ionic liquid thus acts as a "noninnocent" reaction medium at temperatures between 60 and 180 °C. This can take place in one of two different ways. In the first scenario, the imidazolium moiety ("Im") of the ionic liquid releases one of the alkyl groups to become a neutral imidazole ring ("im") that coordinates to a metal atom of the chalcogenido metalate cluster, as observed, for instance, in $(C_4C_1C_1Im)_5[In_{10}Ch_xCl_3(C_4C_1im)]$ (Ch_x = S_{16}; $S_{7.12}Se_{8.88}$; Se_{16}; $Se_{13.80}Te_{2.20}$).[14] In the second scenario, the alkyl group that was released from the imidazolium ring is transferred instead, as observed in salts of a methylated tellurido mercurate cluster anion $(C_nC_1Im)_6[Hg_6Te_6(Te_2)_2(TeMe)_2]$ (**B**, *n* = 6, 8; Me = methyl),[8] in a salt of the ternary selenide cluster, $(dmmpH)_6[Mn_4Sn_4Se_{13}(SeMe)_4]$ (*dmmp* = 2,6-dimethylmorpholine),[8] or in salts of a alkylated oxido-sulfido stannate cluster anion, $(C_4C_1C_xIm)_4[Sn_{10}O_4S_{16}(SR)_4]$ (*x* = 1, 4; R = Me, or R = Bu = butyl).[8,15] The course of the reaction toward one or the other route seems to depend on the respective reaction conditions. In both cases, the resulting clusters show higher solubilities but nearly no effect on the electronic structure and respective optoelectronic properties, as only a small fraction of the metal or chalcogen atoms, respectively, are involved. However, upon butylation, nonpolar functionalization and charge reduction were combined in a way that allowed the cluster-based salts to readily dissolve in standard organic solvents like MeCN or DCM.[15]

We wondered, whether the alkylation of tellurido mercurate cluster anions could also be realized with much longer alkyl chains—knowing that for the porphyrin-like cluster, no functionalization was observed—in order to form lamellar structures containing lower-charged (thus better soluble) cluster anions. We therefore performed a detailed study into the reaction conditions and report the successful ionothermal synthesis of three new tellurido mercurate compounds, two of which comprise functionalized anions while one comprises nonfunctionalized anions, as a function of the respective reactants and reaction conditions, and in which all ions are arranged in lamellar crystal structures.

By the treatment of $Na_2[HgTe_2]$ or $Na_2[Hg_3Te_4]$, respectively, with the long-chain ionic liquid $(C_{10}C_1Im)[BF_4]$, we obtained a compound with a new tellurido mercurate anion exhibiting homoleptic functionalization, $(C_{10}C_1Im)_6[Hg_6Te_6(Te_2)_2(TeDec)_2]$ (**1**); the first known compound comprising a tellurido mercurate anion with heteroleptic functionalization, $(C_{10}C_1Im)_6[Hg_6Te_6(Te_2)_2(TeDec)(TeMe)]$ (**2**); and a salt comprising a related, yet purely inorganic, nonfunctionalized cluster anion, $(C_{10}C_1Im)_4[Hg_4Te_2(Te_2)_2(Te_3)_2]$ (**3**). Further details are provided in the Experimental Section and the Supporting Information. The compounds were structurally characterized by means of single-crystal X-ray diffraction (SC-XRD). The purities of the crystalline solids were determined using powder X-ray diffraction (P-XRD), and the heavy-atom composition was verified by micro-X-ray fluorescence spectroscopy (μ-XRF) on the single crystals used for the SC-XRD experiment.

2. EXPERIMENTAL SECTION

2.1. Syntheses. *2.1.1. General Details.* Due to the sensitivity of some of the starting materials and all of the products toward air and moisture, all reactions and analytical measurements were performed under strict exclusion of air and moisture, using standard Schlenk and glovebox (type Unilab Plus; MBraun) techniques. $Na_2[HgTe_2]$ and $Na_2[Hg_3Te_4]$ were synthesized according to procedures described in the literature.[16,17] $ZnCl_2$ was purchased from Sigma-Aldrich and dried in vacuum. The solvents ethane-1,2-diamine (*en*), MeCN, and *n*-hexane were dried as described in the literature[18] and stored over molecular sieves of pore size 3 or 4 Å under an argon atmosphere. The ionic liquid $(C_{10}C_1Im)[BF_4]$ was purchased from J&K Scientific GmbH or ABCR GmbH and degassed/dried under reduced pressure at around 80 °C for 16 h before use. The general synthesis procedures of compounds **1**−**3** are outlined in detail below.

2.1.2. Synthesis of $(C_{10}C_1Im)_6[Hg_6Te_6(Te_2)_2(TeDec)_2]$ (1). 50 mg (0.10 mmol) of $Na_2[HgTe_2]$, 4 mg (0.03 mmol, 0.3 equiv) of $ZnCl_2$, and 500 mg of $(C_{10}C_1Im)[BF_4]$ were placed in a borosilicate glass ampoule, which was sealed airtight. The ampoule was heated in an oven to 80 °C at a heating rate of 30 °C/h, kept at 80 °C for 24 h, and then cooled down to room temperature at a cooling rate of 10 °C/h. Compound **1** crystallized as thin brownish platelet-shaped crystals in approximately 60% yield. The reported compound $(C_{10}C_1Im)_8[Hg_8Te_8(Te_2)_4]$ (**A**) was also crystallized within this reaction ampoule in approximately 35% yield. Variation of the amounts of $ZnCl_2$ (0.5, 1 equiv) did not alter the identity of the products, but only decreased the overall yield. Other Lewis acid salts were not tested in this study.

2.1.3. Synthesis of $(C_{10}C_1Im)_6[Hg_6Te_6(Te_2)_2(TeDec)(TeMe)]$ (2) and $(C_{10}C_1Im)_4[Hg_4Te_2(Te_2)_2(Te_3)_2]$ (3). 50 mg (0.10 mmol) of $Na_2[Hg_3Te_4]$, 500 mg of $(C_{10}C_1Im)[BF_4]$, and 50 μL of *en* were placed in a borosilicate glass ampoule, which was sealed airtight. The ampoule was heated in an oven to 80 °C at a heating rate of 30 °C/h, kept at 80 °C for 20 h, and then cooled down to room temperature at a cooling rate of 10 °C/h. Compounds **2** and **3** crystallized as thin brownish platelet-shaped crystals and black platelike crystals,

Scheme 2. Survey of Ionothermal Reactions Starting Out from Either $Na_2[HgTe_2]$[16] or $Na_2[Hg_3Te_4]$,[17] Comprising 1D-$\{[HgTe_2]^{2-}\}$ or 2D-$\{[Hg_3Te_4]^{2-}\}$ Anionic Substructures, respectively, to form Molecular Tellurido Mercurate Clusters[a]

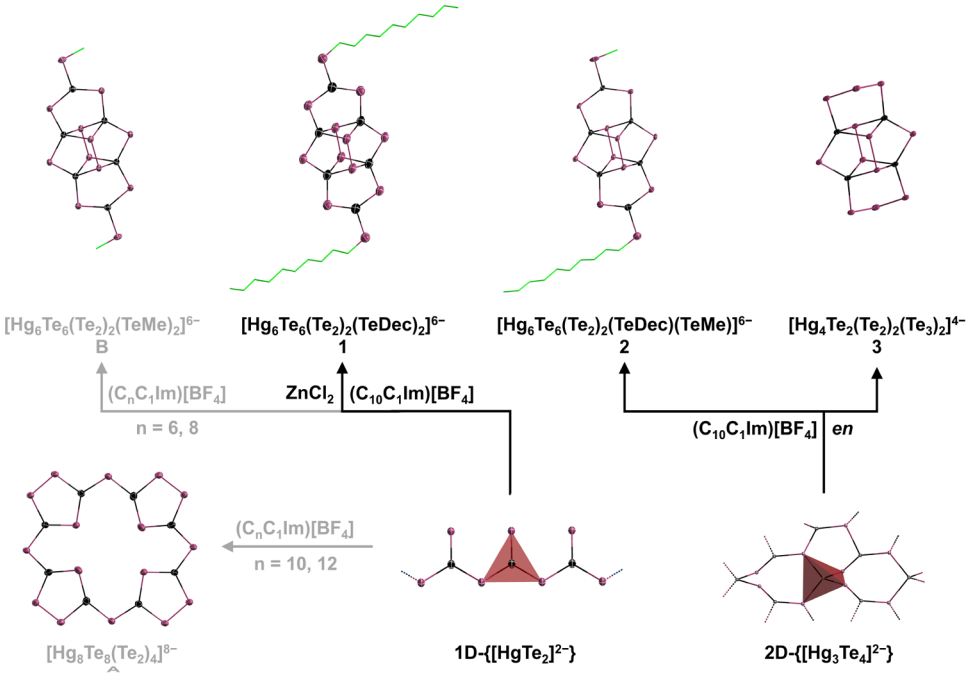

[a]Reaction arrows and formulas belonging to new clusters reported in this work are given in black and those of known ones are given in gray.[7,8] All reactions were carried out at 80 °C

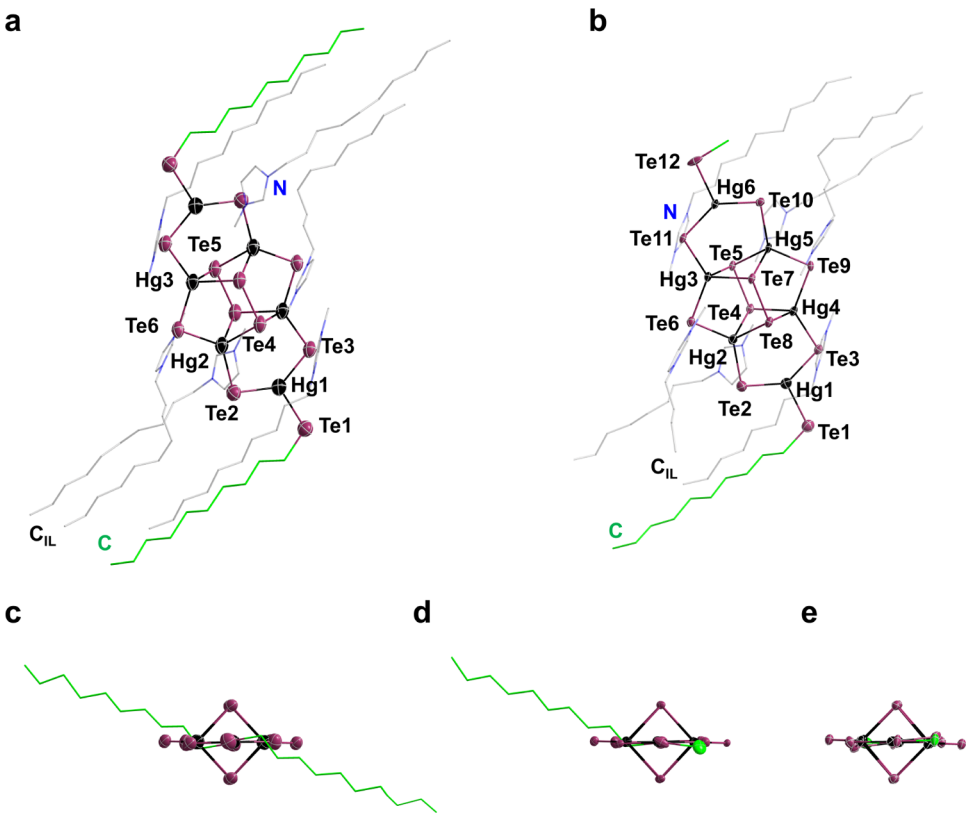

Figure 1. Molecular structures of the hexaanions in compounds **1** (a) and **2** (b) shown along with the six closest counterions each. Hg and Te atoms are drawn as ellipsoids at the 50% probability level. C and N atoms are given in the wire mode and H atoms are omitted for clarity. Alkyl chains of the anionic substructures ("C") are shown in green and those of the imidazolium counterions ("C_{IL}") are drawn in gray. Molecular structures of the anionic substructures of **1** (c), **2** (d), and **B** (e) viewed along the $Te_{terminal}\cdots Te_{terminal}$ axis.

respectively, in a 5:95 ratio and an overall crystalline yield of 90%. Compound **A** was also obtained in the same ampoule in small amounts with a yield of approximately 3%.

The co-formation of **A** is not too surprising, as **1**−**3** form at temperatures of 60−80 °C and at reaction times of at least 12 h, i.e., at temperatures and in time spans that was also reported for the syntheses of **A** and **B** (the latter of which does not seem to form here owing to the apparent preference of a decyl transfer).[7,15] The addition of $ZnCl_2$ or *en*, respectively, seems to cause a shift of the equilibrium that apparently exists in the reaction medium to the main products of this study, **1** and **2**, while they suppress the formation/crystallization of the reported compounds. The synthetic procedures are summarized in Scheme 1.

2.2. Single-Crystal X-ray Diffraction (SC-XRD). Single-crystal diffraction data were collected with Ga Kα radiation (λ = 1.34143 Å) at T = 180 K on the area detector system Stoe StadiVari for compound **1** and with Mo Kα radiation (λ = 0.71073 Å) at T = 100 K on the area detector system Bruker D8 Quest equipped with a CMOS detector for compounds **2** and **3**. The programs X-Area v2.1 (STOE), APEX4 v2021.10-0 (BRUKER), ShelX97, ShelXT15, ShelXL15, XPREP, Olex2 v1.5, and PLATON v90522 were used for the evaluation.[19−23] Crystals were prepared and selected in a *MBraun* MB-10 compact glovebox with a built-in *Leica* M60 reflected light microscope by storing the crystals in NVH immersion oil. Illustrations of the single-crystal structures are provided in Figures 1−5. Measurement, structure solution, and refinement results are detailed in Tables S1−S3 (Supporting Information). Crystallographic data (excluding structure factors) for the structures reported in this paper have been deposited with the Cambridge Crystallographic Data Center as supplementary publication no. CCDC-2264016 (**1**), CCDC-2264017 (**2**), and 2264018 (**3**). Copies of the data can be obtained free of charge on application to CCDC, 12 Union Road, Cambridge CB2 1EZ, UK (fax: (Internet.) +44 1223/336-033 e-mail: depos-it@ccdc.cam.ac.uk). All figures were generated with Diamond v4.6.8.[24]

2.3. Powder X-ray Diffraction (P-XRD). P-XRD data were obtained with Cu Kα radiation (λ = 1.54060 Å) in transmission mode on a Stoe StadiMP diffractometer using a highly sensitive Mythen detector system and a curved focusing monochromator. The samples were prepared in a glovebox by sealing a small amount of crystalline powder tightly with scotch tape and clamping it on a transmission carrier. The transmission carrier was then brought to the device in a tightly closed container (shuttle) to minimize the dwell time in air (limited to 5−10 s until measurement). The maximum duration of the measurement was 15 min per sample. The data examination was done using WinXPOW v3.11 and OriginPro 2023, and the P-XRD diagrams are shown in Figure 6.

2.4. Micro-X-ray Fluorescence Spectroscopy (μ-XRF). The μ-XRF analyses were performed using a Bruker Tornado M4 spectrometer. Single-crystal samples were fixed on the sample holder with small amounts of NVH immersion oil. Rhodium and tungsten X-ray tubes served as radiation sources. The detector system consisted of two energy-dispersive XFlash X-ray detectors based on the SDD (silicon drift detector) principle with an internal FET (field-effect transistor). Measurements were performed at approximately 2 mbar unless otherwise specified. Fluorescence emission was recorded at measurement times of 180 or 240 s. Quantification was based on Te-*L* and Hg-*L* fluorescence radiation. The percentages are the substance amount concentration in atomic%. The evaluation was performed with the program Esprit. The spectra are shown in Figures S8−S10, and the results are summarized in Tables S4−S6.

2.5. Infrared (IR) Spectroscopy. Infrared spectra of **1** and **3** were recorded on a Bruker ALPHA II IR spectrometer with an ATR platinum measurement unit. Raw data were processed using OriginPro 2023. Intensities of the transmitted bands are given as follows: vw (very weak), w (weak), m (medium), s (strong), vs (very strong), and b (broad). The spectra are shown in Figure 7a (for more details, see the Supporting Information, Figures S11 and S12).

2.6. Raman Spectroscopy. Raman spectra were acquired using an inVia Raman microscope (Renishaw; Wotton-under-Edge, Gloucestershire, United Kingdom). A 20× objective was used to align/center the sample. The excitation wavelength was 532 nm, and measurements were performed with a laser power of 1%. The sample was irradiated three times for 60 s, and the individual measured spectra were accumulated into a total spectrum. Raw data were processed using OriginPro 2023. Intensities of the transmitted bands are given as follows: vw (very weak), w (weak), m (medium), s (strong), vs (very strong), and b (broad). The spectrum is shown in Figure 7b (for more details, see the Supporting Information, Figure S13).

2.7. UV−Visible (UV−vis) Spectroscopy. Optical absorption spectra of compounds **1** and **3** were measured in diffuse-reflectance mode on single crystals, employing a Varian Cary 5000 UV/VIS/NIR spectrometer from Agilent, equipped with a Praying Mantis accessory for the solid-state samples. Tauc plots were generated using the Kubelka−Munk function $(F(R_\infty)h\nu)^{1/\gamma}$, with γ = 1/2, indicative for a direct allowed optical gap, or γ = 2, indicative for an indirect allowed optical gap.[25−27] The spectra are shown in Figure 8 (for more details, see the Supporting Information, Figure S14).

3. RESULTS AND DISCUSSION

3.1. Syntheses. As illustrated in Scheme 1, the three title compounds were synthesized by treating $Na_2[HgTe_2]$[16] or $Na_2[Hg_3Te_4]$,[17] respectively, with the ionic liquid $(C_{10}C_1Im)[BF_4]$, similar to the reactions reported for the synthesis of the salt of porphyrin-like cluster anion **A**.[7] For compound **1**, in a first variation of the reaction conditions, we used $Na_2[HgTe_2]$ with small amounts of $ZnCl_2$ (0.3 equiv.), thereby increasing the Lewis acid nature of the reaction mixture, which seems to affect the cluster formation processes in a yet unclarified way. Without using $ZnCl_2$, **A** is obtained as the main product, with small amounts of **1** as the byproduct. Compound **1** is obtained in higher crystal quality and yield in the presence of $ZnCl_2$, possibly because the Lewis acid Zn^{2+} ions assist in the Hg−Te framework reconstruction by breaking bonds in the 1D chains of $Na_2[HgTe_2]$ and forming new bonds to build the molecular architecture. This seems to be more preferable for the formation of the more spherical cluster in **1**. Upon using another starting material, $Na_2[Hg_3Te_4]$, and adding small amounts of the base ethane-1,2-diamine (*en*), compounds **2** and **3** are obtained together. In addition to **2** and **3**, compound **A** also co-crystallizes in very low yield in the reaction ampoule. The main product in this reaction is compound **2**, while **3** and **A** are only obtained in traces of a few crystals per batch (thus, not detectable by P-XRD, see Figure 6 in Section 3.3).

3.2. Crystal Structures. The inorganic core structure of **1** and **2** is the same as for **B**, which was obtained by treatment of $Na_2[HgTe_2]$ in ionic liquids with shorter alkyl chains, such as $(C_6C_1Im)[BF_4]$ and $(C_8C_1Im)[BF_4]$, and which represented the first organically decorated tellurido mercurate cluster anion.[8] While decylation is found on both terminal Te atoms in **1**, there is a methyl substituent on one terminal Te atom and a decyl substituent on the other in **2**. Both functionalized groups originate from the ionic liquid cation, which is reactive enough to donate its alkyl chains to the cluster anion. This is the first case in which an imidazolium ion transferred both alkyl groups instead of selectively transferring one of them only, but the very low yield of **2** indicates that the release of the methyl group is not preferred. The anionic substructure of **3** was first observed in $[n\mathrm{Bu_4N}]_4[Hg_4Te_2(Te_2)_2(Te_3)_2]$ upon an aminothermal reaction of $K_2[Hg_2Te_3]$ in *en* with a MeOH solution of $[n\mathrm{Bu_4N}]Br$.[28] In **3**, however, another cation is present that causes the crystal structure to exhibit a lamellar pattern as desired. Compound **3** is an inorganic, not alkyl-

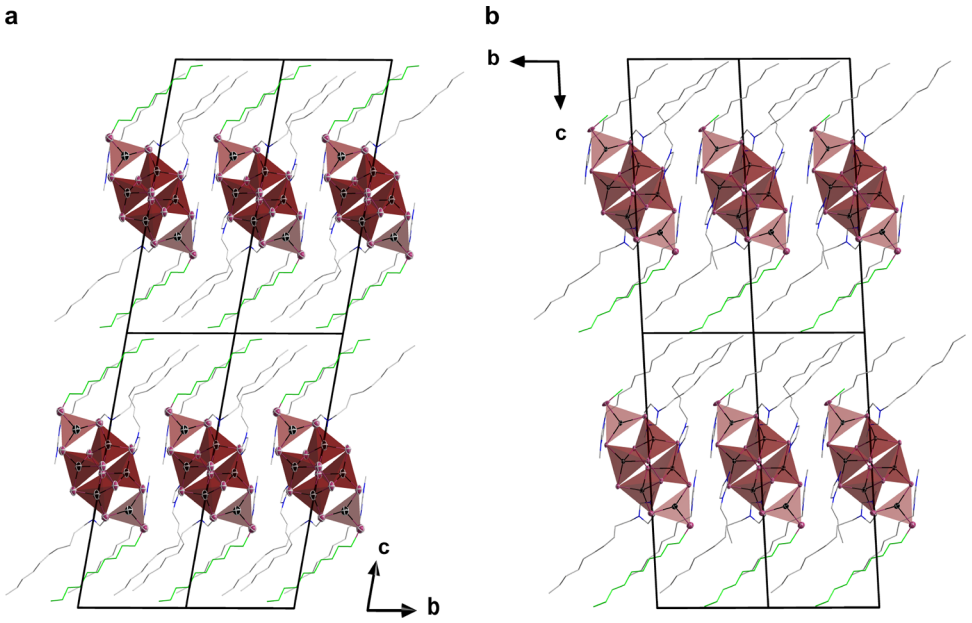

Figure 2. Representation of 2 × 2 × 2 supercells of the crystal structures of compounds **1** (a) and **2** (b), viewed along crystallographic *a*-axis to illustrate and compare their lamellar crystal structures. Hg and Te atoms are drawn as ellipsoids at the 50% probability level; C and N atoms are given in the wire mode; alkyl chains are shown as wires—green at the cluster and gray at the counterions. The Hg/Te cores of the anions are highlighted in polyhedral representation; H atoms are omitted for clarity. Color code: Hg = black, Te = plum, C = green or gray, and N = blue.

functionalized, analogue of **1** and **2**. Scheme 2 summarizes the results obtained in this study and also indicates related synthetic procedures leading to similar products that were previously reported.

As mentioned above, the anionic substructures observed in **1** and **2** are similar to that of the methylated tellurido mercurate cluster in **B**. The anions of **1** and **2** thus consist of four (distorted) tetrahedral $[HgTe_4]^{6-}$ units (τ_4 = 0.87−0.89 in **1** and **2**; τ_4 = 0.84−0.89 in **B**; τ_4 indicates the geometric deviation of an arrangement from an ideal tetrahedron, τ_4 = 1, or a planar square, τ_4 = 0[29]) and two trigonal planar $[HgTe_3]^{4-}$ units (angle sums of ≥ 359.994(5)° in **1** and **2**; ≥ 359.35(2)° in **B**), with the organic groups in **1** and **2** attached to the two terminal telluride ligands. This results in a charge reduction from that of an (yet unknown) underlying cluster without organic groups (−8) to −6 in the compounds reported herein. An even lower charge (−4) is found in the $[Hg_4Te_2(Te_2)_2(Te_3)_2]^{4-}$ cluster anion of **3** upon (formal) replacement of two $[HgTe_3C_x]^{3-}$ units (x = 1 and/or 10) with two Te_3^{2-} fragments. Compound **3** is a rare case in which a cluster is formed under ionothermal conditions that has previously been obtained by other ways, namely, by solution-based approaches, like $[n\mathrm{Bu}_4\mathrm{N}]_4[Hg_4Te_2(Te_2)_2(Te_3)_2]$ and $[NMe_4]_4[Hg_4Te_2(Te_2)_2(Te_3)_2]$ (**C**).[29,31] The accessible volume between the anionic clusters in the crystals of all three compounds is filled with the counterions, i.e., the ionic liquid cations $(C_{10}C_1Im)^+$.

Compound **1** crystallizes as thin, platelet-like brownish crystals in the triclinic crystal system, space group $P\bar{1}$ (No. 2), with one formula unit per unit cell (V = 3428.2(7) Å^3), and compound **2** crystallizes as thin, platelet-shaped brownish crystals in the triclinic crystal system, space group $P1$ (No. 1), with one formula unit per unit cell (V = 3287.3(4) Å^3). The cluster anion in **1** is centered on a crystallographic inversion center, which is not the case for the anion in **2** owing to its unsymmetrical substitution pattern, which also comes along with an unsymmetrical location of the counterions. However, in both clusters, the Hg/Te substructures show a high (idealized D_{2h}) symmetry. All heavy atoms—except those of the $\{Te_2\}$ units—lie in one plane (with the root-mean-square deviation of the atoms from a mean plane of all heavy atoms—except for the $\{Te_2\}$ units—being 0.049 Å for cluster **1** and 0.041 Å for cluster **2**). Notably, the alkyl groups of the cluster anions in **1** and **2** (Figure 1a,b) do not arrange in that plane, in contrast to the relative orientation of the two methyl groups in **B** (Figure 1c−e). Furthermore, unlike in **B**, the crystal structures of **1** and **2** feature a lamellar arrangement of the anionic cluster cores and imidazolium rings of the cations between layers comprising the alkyl chains of the clusters and of the counterions. This can be explained by the fact that the alkyl "chain" (i.e., a Me group) at both the cation and the anion in **B** is not long enough. The bond lengths in **1** [Hg−Te: 2.667(2)−2.795(2) Å, Hg−$\{Te_2\}$: 2.936(2)−2.960(2) Å, Te−Te: 2.740(2) Å] and in **2** [Hg−Te: 2.665(3)−2.800(2) Å, Hg−$\{Te_2\}$: 2.925(3)−2.989(3) Å, Te−Te: 2.727(3)−2.742(3) Å] are in good agreement with those of the related $[Hg_6Te_6(Te_2)_2(TeMe)_2]^{6-}$ anion in **B** [Hg−Te: 2.654(4)−2.814(3) Å, Hg−$\{Te_2\}$: 2.940(1)−2.949(1) Å, Te−Te: 2.734(1) Å]. The same holds for the bond angles (see Table S7). The Te−C bonds in **1** (2.130(4) Å) and **2** (2.130(2) for Te−C_{10} and 2.230(3) Å for Te−C_1) are similar to those observed in **B** (2.174(3)−2.187(5) Å); the somewhat broader range observed in **2** is attributed in part to the disorder.

The views of the 2 × 2 × 2 supercells along the crystallographic *a*-axis (Figure 2) illustrate the lamellar crystal structures, in which polar and nonpolar layers are arranged alternately. In these layered structures, the anions are surrounded by the imidazolium rings of six closest counterions each (polar layer), while the alkyl groups (mainly the decyl substituents) of the anions $[Hg_6Te_6(Te_2)_2(TeC_x)_2]^{6-}$ (x = 1 and/or 10) undergo van der Waals interactions with the long-chain alkyl substituents of the $(C_{10}C_1Im)^+$ cations (nonpolar

layer). The way in which the decyl chains (from the clusters and also from the counterions) are interlocked differs in two regards from that observed in **A**,[7] where the nonpolar layers were formed by the cations only. First, the relative orientation of the alkyl chains is less regular and not equidistant in **1** and **2**—also because both cations and anions are involved. Second, the nonpolar layers are separated into double layers here, with no interlocking of alkyl chains of one "cluster plus counterion" layer with those of the adjacent one. This is likely to result in weaker overall van der Waals interactions than, e.g., in compound **A** with the porphyrin-related anions[7] and hence represents a promising prerequisite for attempting to exfoliate single crystals of these compounds and to prepare monolayers of the imidazolium salts. Efforts to do so by mechanical exfoliation using a tape have failed so far; methods using liquids, which are challenging owing to the high anionic charge, are currently under investigation.

Compound **3** crystallizes as black platelike crystals in the triclinic crystal system, space group $P\bar{1}$ (No. 2), with two formula units per unit cell (V = 4112.9(1) Å^3). The cluster anion in **3** consists of an inversion-symmetric $[Hg_4(Te_2)_2Te_2]$ core with two terminal Te_3^{2-} "handles". Four Hg atoms are coordinated in a distorted tetrahedral manner (τ_4 = 0.81−0.88 in **3**; τ_4 = 0.83 in **C**[30]) by tellurium atoms that stem from three different types of subunits: two Te^{2-}, two Te_2^{2-}, and two Te_3^{2-}. The center of the $[Hg_4Te_{12}]^{4-}$ cluster also contains the crystallographic inversion center. Figure 3 shows the molecular

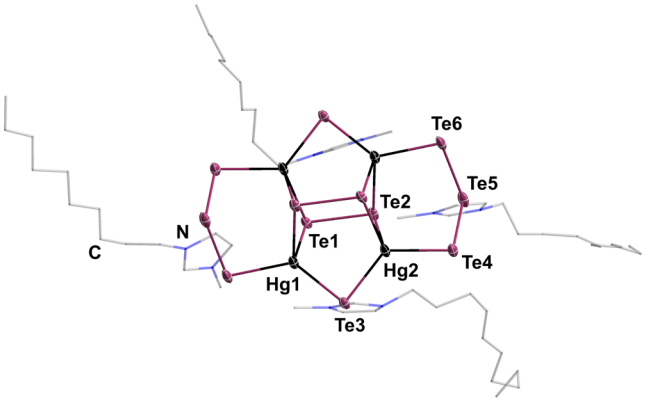

Figure 3. Molecular structure of the tetra anion in compound **3** shown along with the four closest counterions. Hg and Te atoms are drawn as ellipsoids at the 50% probability level; C and N atoms are given in the wire mode; the heavily disordered part of the cations and H atoms are omitted for clarity.

structure of the anion and the counterions (without disorder; for more details, see the Supporting Information). All bond lengths in **3** [Hg−Te: 2.700(7)−2.729(7) Å, Hg−{Te_2}: 2.889(8)−3.029(8) Å, Hg−{Te_3}: 2.744(8)−2.801(7) Å, Te−Te: 2.710(9)−2.744(8) Å] accord well with those found in the $[Hg_4Te_{12}]^{4-}$ anion in **C** [Hg−Te: 2.713(4)−2.717(3) Å, Hg−{Te_2}: 2.931(3)−2.984(4) Å, Hg−{Te_3}: 2.777(3)−2.794(4) Å, Te−Te: 2.719(4)−2.739(4) Å]. The same applies to the bond angles (see Table S8).[30]

While the molecular structure of the anion in **3** is widely identical with the anionic substructure of the known compound **C**, a view of the 2 × 2 × 2 supercell of **3** (Figure 4) indicates a fundamental difference: as described above for new compounds **1** and **2**, the ions in **3** are arranged in a lamellar mode, in which polar and nonpolar layers alternate.

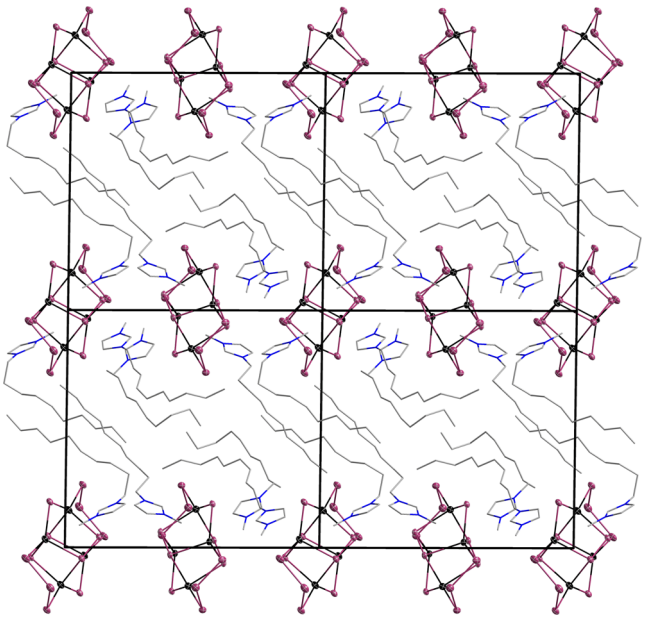

Figure 4. Representation of the 2 × 2 × 2 supercell of the crystal structure of compound **3** viewed along the crystallographic *a*-axis to highlight its lamellar crystal structure. Hg and Te atoms are drawn as ellipsoids at the 50% probability level; C and N atoms are given in the wire mode; H atoms are omitted for clarity. Color code: Hg = black, Te = plum, C = gray, and N = blue.

Again, the $[Hg_4Te_2(Te_2)_2(Te_3)_2]^{4-}$ anion is surrounded by the imidazolium rings (polar part), while the alkyl chains of (only) the cation form the nonpolar layer separating the polar one from each other. However, as illustrated by a view of the 2 × 2 × 2 supercell, the decyl chains of the counterions in **3** are arranged in a much more random manner and not aligned as in **1** and **2**. This results in a shorter length of the corresponding unit cell axis perpendicular to the layers, the *b* axis in **3**.

We compared the interlayer spacings,[5,6] defined as the distance between the polar layers, in the lamellar crystal structures of compounds **1**−**3** and **A**.[7] These vary notably, although all four compounds feature decyl chains at the imidazolium cation, which can be put down to the different orientation of the decyl groups relative to the Hg/Te cluster cores, as illustrated in Figure 5.

The interlayer spacing is the largest in **A** (17.7 Å),[7] in accordance with a straight orientation of all decyl groups between the polar layers. In contrast to the structure of **A** (and as mentioned above), the decyl chains above and beneath the polar layers in **1** and **2** do not interfere but form a double layer with a small spacing between these two nonpolar layers (2.84 Å in **1**; 1.14 Å in **2**); hence, one might assume that the interlayer spacing would be larger than in **A**. However, a significant tilt of the chains relative to the longest axis of the cluster anions (running from one terminal Te atom to the other), thus also relative to the polar layers, allows the polar layers to approach. The resulting interlayer spacing values are thus 17.1 Å in **1** and 15.8 Å in **2**. The slight decrease from **1** to **2** correlates with the replacement of 50% of the decyl groups on the cluster with methyl groups, which causes the clusters to pack a bit denser; this also affects the optical absorption properties (see Section 3.4 and Figure 8 below). The smallest interlayer spacing is observed in compound **3** (9.55 Å). This is due to a lack of alkyl chains on the clusters (thus fewer atoms in the unit cells) and comes along with a rather random

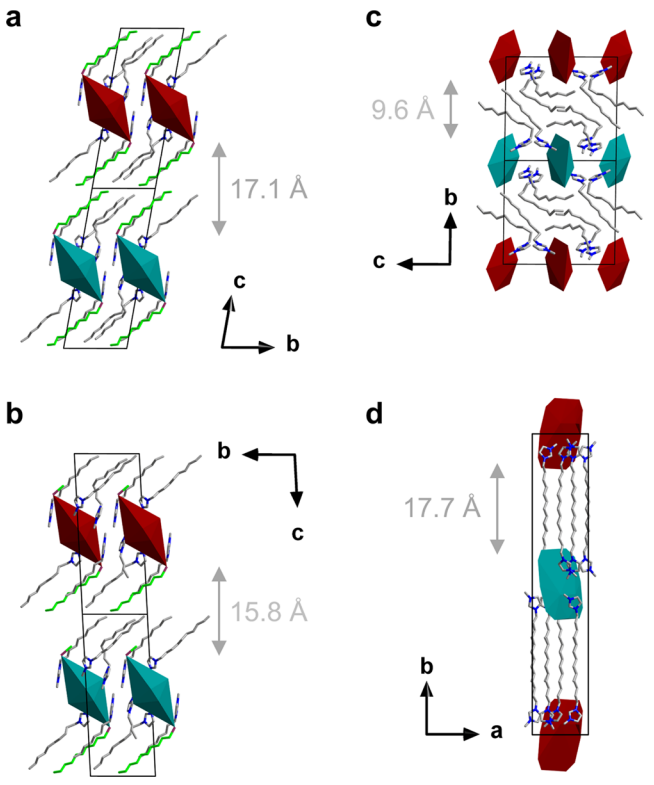

Figure 5. Comparison of the interlayer spacing in the lamellar structures of compounds **1**–**3** (a–c) and **A** (d). The anionic substructures are simplified in the polyhedral mode in two different colors representing different layers, and the cations are shown as bold wires.

orientation of the alkyl chains of the counterions with apparently no order. Very obviously, the different cluster types affect the nature of the lamellar arrangement of the cations, indicating the flexibility of such compounds.

3.3. Powder X-ray Diffraction (P-XRD). Powder diffraction was performed on the content of the reaction ampoules of **1** and **2**/**3** to investigate the purity of the reaction products and to confirm the identity of the compounds in the bulk material. Figure 6 gives the diffractogram of **1** (black line) in comparison with the simulation from SC-XRD data (red line) and opposed to that of compound **A** (blue line).

For compound **1** (see Figure 6a), the experimental and the simulated diffraction patterns correlate very well with each other. Slight deviations are based on different temperatures applied for the P-XRD measurement (room temperature; SC-XRD: 100 K) and on texture effects owing to the thin platelike nature of the crystals, which can cause reflections to be absent or intensities to deviate. A few reflections (around 6, 10, and 23°) stem from traces of co-forming compound **A** (see above), which could not be removed. The higher background is due to the adherent ionic liquid on the crystalline residue.

The diffraction pattern that was obtained for the product mixture of compounds **2** and **3** was compared with the P-XRD pattern simulated from the SC-XRD data of **3** (measured at room temperature), see Figure 6b. Compound **3** is the only detectable compound and thus represents the main product of the reaction. Some minor discrepancies, like missing reflections and modified intensities, again are due to the platelike nature of the crystals and the co-formation of small amounts of compounds **2** and **A**.

3.4. Vibrational and Optical Absorption Properties. For further characterization of title compounds, and for getting more insight into the influence of the different molecular and crystal structures on the properties of the compounds, we performed vibrational (IR and Raman) and optical absorption (UV–visible) spectroscopy. For determining the effect of the organic decoration of the cluster anions in general, we restricted our analysis on the comparison of compound **1** (with organic groups) and compound **3** (without organic groups); note that the low yield of compound **2** besides co-forming compound **3** prohibited further analyses of the former in the pure form.

Figure 7a shows the IR spectra recorded on pulverized (manually selected) single crystals of compounds **1** (blue line) and **3** (orange line). Both compounds show very similar vibrational modes, which mainly differ in their relative intensities. However, the differences are clearly there and correlate with minor differences in bond lengths, slightly

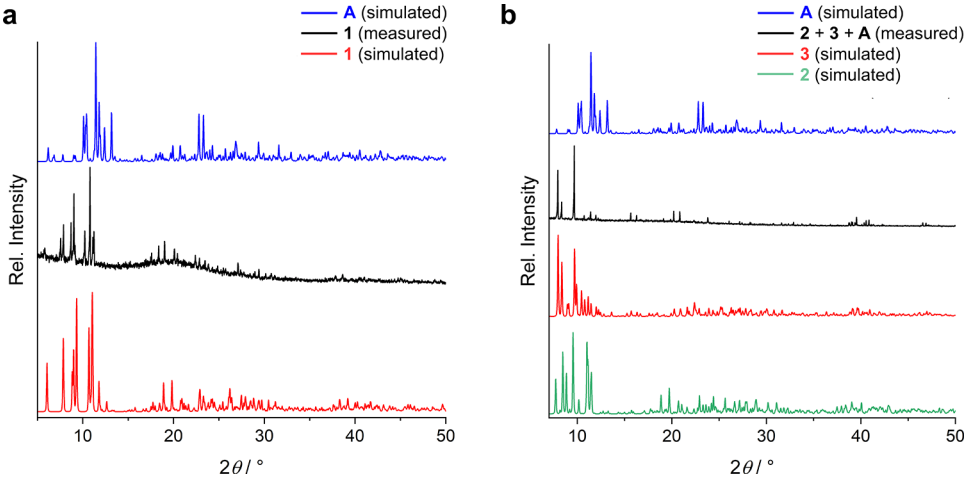

Figure 6. Experimental P-XRD pattern of compound **1** (black line), in comparison with the P-XRD patterns simulated from the corresponding SC-XRD structure (red line, simulated based on SC-XRD data) and that of **A** (blue line, simulated based on SC-XRD data) (a). Experimental P-XRD pattern of the reaction mixture comprising compounds **2**, **3**, and **A** (black line), compared to the simulated P-XRD patterns of **3** (red line, simulated based on SC-XRD data), **2** (green line, simulated based on SC-XRD data), and **A** (blue line, simulated based on SC-XRD data) (b).

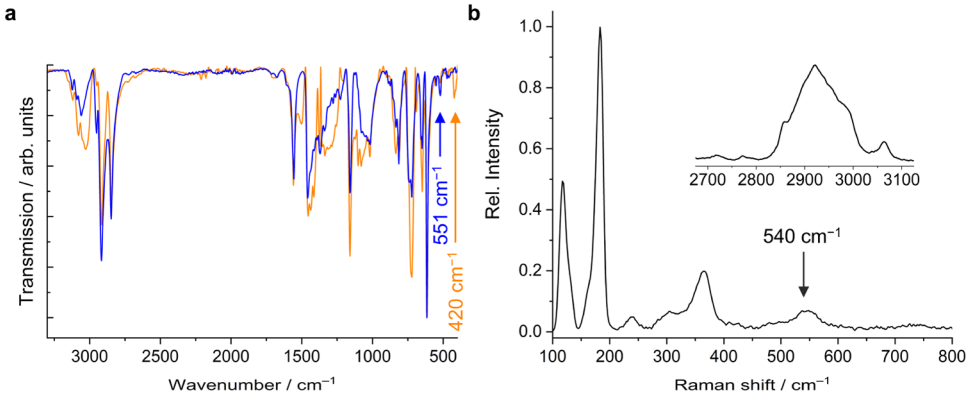

Figure 7. Infrared spectrum (a) of compound **1** (blue line) compared to **3** (orange line). Raman spectrum of **1** (b).

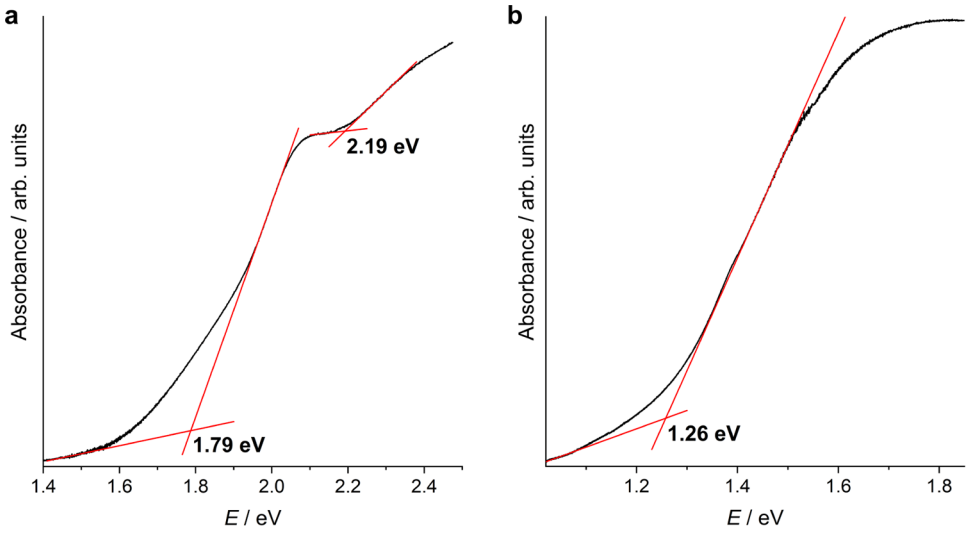

Figure 8. Comparison of the solid-state UV−visible diffuse-reflectance spectra of **1** (a) and **3** (b).

different symmetries of the cluster cores, and the presence of organic substituents in **1** versus polytelluride units in **3**. The bands in the range of 2800−3200 cm^{-1} and the bands at about 1500 and 1000 cm^{-1} can be attributed to the ionic liquid cations (C−H valence vibrations and imidazolium ring vibrations). Below 1000 cm^{-1}, we observe bands representing the C−H deformation vibrations. The band observed in the spectrum of **1** at 551 cm^{-1} is of particular interest, as it corresponds to Te−C vibrations and therefore need to be absent in the spectrum of **3**, which is the case. Comparisons with the Te−C vibrational modes reported for Me_2Te (504 cm^{-1}) and tBu_2Te (498 cm^{-1}) show good agreement.[31] The differences arise from the different coordination environments of the Te atoms and different Te−C bond lengths resulting from them. The group of bands at around 420 cm^{-1}, only present in the spectrum of **3**, is indicative of the vibrations of the polytelluride units attached to the cluster anion. Hence, the IR spectra are a suitable means of providing fingerprints for purely inorganic versus organyl-functionalized tellurido mercurate clusters.

Additional evidence of the organic functionalization of the cluster anion in **1** is provided by Raman spectra recorded on single crystals (Figure 7b). The spectrum exhibits the characteristic signal groups of the cluster core between 100 and 400 cm^{-1}, while the signal groups at 540 cm^{-1} and at around 2900 cm^{-1} are assigned to the Te−C bond and the bonds within the imidazolium cations as well as the decyl groups of the cluster—in good agreement with reported data.[31]

In order to investigate the band gap energies and the nature of the electronic transitions that take place in these different types of lamellar structures, we performed UV−visible spectroscopy on pulverized single crystals of compounds **1** and **3**. The spectra were recorded in diffuse-reflectance mode, and the data were converted into Tauc plots using the Kubelka−Munk function.[25−27] $(F(R_\infty)h\nu)^{1/\gamma}$ was plotted as a function of the photon energy; γ as the power coefficient corresponds to the type of the transition (γ = 0.5: directly allowed; γ = 2: indirectly allowed). Additionally, the spectra measured in diffuse-reflectance mode were transformed into absorbance spectra (Figure 8).

The spectrum of **1** shows two absorptions, one of which, at 1.79 eV (693 nm), represents the main onset of absorption, indicative of the optical band gap of compound **1** in accordance with the visible brownish color of the crystals. A shoulder at 2.19 eV (566 nm) is likely due to polytelluride decomposition products (typically showing red colors) which form by partial oxidation of the telluride ligands during the measurements of this very sensitive compounds or the presence of traces of co-forming compound **A** (reported band gap 2.16 eV, 574 nm) in the sample.[7] The UV−vis spectrum of **3** shows a main band gap at about 1.26 eV (984

nm), which again is in agreement with the visible black appearance of this compound. Although the inorganic cluster in **3**, $[Hg_4Te_2(Te_2)_2(Te_3)_2]^{4-}$, contains fewer Hg atoms than the $[Hg_6Te_6(Te_2)_2(TeDec)_2]^{6-}$ cluster in **1**, the replacement of terminal tellurolate ligands with the polytelluride units and the concomitant denser packing of the clusters in the salt lead to a shift of the band gap to lower energies. Unfortunately, optical gaps of the related compounds, $[nBu_4N]_4[Hg_4Te_2(Te_2)_2(Te_3)_2]$[28] and $[NMe_4]_4[Hg_4Te_2(Te_2)_2(Te_3)_2]$ (**C**),[30] had not been reported; therefore, a comparison is not possible.

The importance of the density of the inorganic chromophores in the crystals is evident, when comparing the band gaps of **1** and **3** with that of **A** (2.16 eV).[7] In spite of a larger, purely inorganic cluster molecule, $[Hg_8Te_8(Te_2)_4]^{8-}$, also comprising ditelluride units, the optical absorption bands of the new compounds are significantly red-shifted owing to the significantly smaller interlayer spacing discussed above.

The Tauc plots of **1** and **3** (Figure S14) indicate that the main transition at 1.79 eV is of an indirectly allowed nature (and that of the subsequent transition at 2.19 eV, too). The transition detected for **3** at 1.26 eV is also of an indirectly allowed nature according to the Tauc plot.

4. CONCLUSIONS

In summary, we have exploited ionothermal reactions with noninnocent ionic liquids to form two new functionalized tellurido mecurate anions, one with homoleptic decylation of the tellurido mercurate cluster anion (in **1**) and another one with heteroleptic functionalization of a tellurido mercurate cluster anion by one methyl and one decyl group (in **2**). Both compounds exhibit lamellar crystal structures as a consequence of long alkyl chains being present on the cluster anions and the ionic liquid cations that serve for charge compensation in the salts—however with smaller interlayer spacing than previously observed for the salt of the inorganic porphyrin analogue **A**.[7] Besides these two compounds, we obtained a related cluster without organic decoration (in **3**), which also forms a lamellar crystal structure together with the counterions. IR/Raman spectra confirmed the presence of the decyl groups in **1** and of the tritelluride unit in **3**. The optical absorption spectra of **1** and **3** reflect the different content of polytellurides in the compounds, and the spectra allowed the determination of the influence of the different interlayer spacing in salts of organyl-decorated tellurido mercurate clusters and purely inorganic ones on electronic properties.

ASSOCIATED CONTENT

Accession Codes

CCDC 2264016–2264018 contain the supplementary crystallographic data for this paper. These data can be obtained free of charge via www.ccdc.cam.ac.uk/data_request/cif, or by emailing data_request@ccdc.cam.ac.uk, or by contacting The Cambridge Crystallographic Data Centre, 12 Union Road, Cambridge CB2 1EZ, UK; fax: +44 1223 336033.

Crystallographic Information Files of compounds **1**–**3** (CIF).

AUTHOR INFORMATION

Corresponding Author

Stefanie Dehnen − *Institute of Nanotechnology (INT), Karlsruher Institute of Technology (KIT), 76344 Eggenstein-Leopoldshafen, Germany;* orcid.org/0000-0002-1325-9228; Email: stefanie.dehnen@kit.edu

Authors

Mirko Tallu − *Institute of Nanotechnology (INT), Karlsruher Institute of Technology (KIT), 76344 Eggenstein-Leopoldshafen, Germany*

Bertram Peters − *Fachbereich Chemie and Wissenschaftliches Zentrum für Materialwissenschaften, Philipps-Universität Marburg, 35043 Marburg, Germany*

Alexander Friedrich − *Fachbereich Chemie and Wissenschaftliches Zentrum für Materialwissenschaften, Philipps-Universität Marburg, 35043 Marburg, Germany*

Author Contributions

The manuscript was written through contributions of all authors. All authors have given approval to the final version of the manuscript.

Notes

The authors declare no competing financial interest.

ACKNOWLEDGMENTS

The authors thank Dr. Sergei Ivlev and Dr. Radostan Riedel from the X-ray service department of Philipps-Universität Marburg and Prof. Dr. Dieter Fenske from the Institute of Nanotechnology of KIT for their help with single-crystal X-ray diffraction experiments. The authors also thank Dr. Vanessa Miß for SC-Raman spectroscopy measurements. The authors gratefully acknowledge financial support from the Deutsche Forschungsgemeinschaft (DFG, German Research Foundation) and support by the Karlsruhe Nano Micro Facility (KNMFi).

REFERENCES

(1) Gorter, E.; Grendel, F. On Bimolecular Layers of Lipoids on the Chromocytes of the Blood. *J. Exp. Med.* **1925**, *41*, 439.

(2) Li, J.; Marler, B.; Kessler, H.; Soulard, M.; Kallus, S. Synthesis, Structure Analysis, and Characterization of a New Thiostannate, $(C_{12}H_{25}NH_3)_4[Sn_2S_6]\cdot 2H_2O$. *Inorg. Chem.* **1997**, *36*, 4697–4701.

(3) Bonhomme, F.; Kanatzidis, M. G. Structurally Characterized Mesostructured Hybrid Surfactant-Inorganic Lamellar Phases Containing the Adamantane $[Ge_4S_{10}]^{4-}$ Anion: Synthesis and Properties. *Chem. Mater.* **1998**, *10*, 1153–1159.

(4) Wachhold, M.; Kanatzidis, M. G. Surfactant-Templated Inorganic Lamellar and Non-Lamellar Hybrid Phases Containing Adamantane $[Ge_4Se_{10}]^{4-}$ Anions. *Chem. Mater.* **2000**, *12*, 2914–2923.

(5) Rangan, K. K.; Kanatzidis, M. G. Mesolamellar Thiogermanates $[C_nH_{2n+1}NH_3]_4Ge_4S_{10}$. *Inorg. Chim. Acta* **2004**, *357*, 4036–4044.

(6) Suh, M. J.; Vien, V.; Huh, S.; Kim, Y.; Kim, S. J. Mesolamellar Phases Containing $[Re_6Q_8(CN)_6]^{4-}$ (Q = Te, Se, S) Cluster Anions. *Eur. J. Inorg. Chem.* **2008**, *2008*, 686–692.

(7) Donsbach, C.; Reiter, K.; Sundholm, D.; Weigend, F.; Dehnen, S. $[Hg_4Te_8(Te_2)_4]^{8-}$: A Heavy Metal Porphyrinoid Embedded in a Lamellar Structure. *Angew. Chem., Int. Ed.* **2018**, *57*, 8770−8774.
(8) Peters, B.; Santner, S.; Donsbach, C.; Vöpel, P.; Smarsly, B.; Dehnen, S. Ionic Liquid Cations as Methylation Agent for Extremely Weak Chalcogenido Metalate Nucleophiles. *Chem. Sci.* **2019**, *10*, 5211−5217.
(9) Donsbach, C.; Dehnen, S. Formation of $[(C_nC_1imTe)_4Hg]^{2+}$ (n = 6, 8) upon in-situ Generation of Dialkylimidazole-2-Tellurones in Ionic Liquids at Room Temperature. *Eur. J. Inorg. Chem.* **2018**, *2018*, 4429−4433.
(10) Peng, Y.; Hu, Q.; Liu, Y.; Li, J.; Huang, X. Discrete Supertetrahedral Tn Chalcogenido Clusters Synthesized in Ionic Liquids: Crystal Structures and Photocatalytic Activity. *ChemPlusChem* **2020**, *85*, 2487−2498.
(11) Wu, Z.; Stuhrmann, G.; Dehnen, S. Crystalline Chalcogenidometalate-Based Compounds from Uncommon Reaction Media. *Chem. Commun.* **2022**, *58*, 11609−11624.
(12) Xiong, W.-W.; Li, J.-R.; Hu, B.; Tan, B.; Li, R.-F.; Huang, X.-Y. Largest Discrete Supertetrahedral Clusters Synthesized in Ionic Liquids. *Chem. Sci.* **2012**, *3*, 1200−1204.
(13) Du, C. F.; Shen, N. N.; Li, J. R.; Hao, M. T.; Wang, Z.; Huang, X. Y. Synthesizing 2D and 3D Selenidostannates in Ionic Liquids: The Synergistic Structure-Directing Effects of Ionic Liquids and Metal−Amine Complexes. *Chem. − Asian J.* **2016**, *11*, 1555−1564.
(14) Shen, N. N.; Hu, B.; Cheng, C. C.; Zou, G. D.; Hu, Q. Q.; Du, C. F.; Li, J. R.; Huang, X. Y. Discrete Supertetrahedral T3 InQ Clusters (Q = S, S/Se, Se, Se/Te): Ionothermal Syntheses and Tunable Optical and Photodegradation Properties. *Cryst. Growth Des.* **2018**, *18*, 962−968.
(15) Peters, B.; Stuhrmann, G.; Mack, F.; Weigend, F.; Dehnen, S. Highly Soluble Supertetrahedra upon Selective Partial Butylation of Chalcogenido Metalate Clusters in Ionic Liquids. *Angew. Chem., Int. Ed.* **2021**, *60*, 17622−17628.
(16) Donsbach, C.; Dehnen, S. Formation of Crystalline Telluridomercurates from Ionic Liquids near Room Temperature. *Z. Anorg. Allg. Chem.* **2017**, *643*, 14−19.
(17) Li, J.; Chen, Z.; Lam, K. C.; Mulley, S.; Proserpio, D. M. $Rb_2Hg_3Te_4$: A New Layered Compound Synthesized from Solvothermal Reactions. *Inorg. Chem.* **1997**, *36*, 684−687.
(18) Armarego, W. L. F.; Chai, C. L. L. *Purification of Laboratory Chemicals*, 6th ed.; Butterworth-Heinemann Ltd.: Burlington, 2009; p 760.
(19) Sheldrick, G. M. SHELXT − Integrated space-group and crystal-structure determination. *Acta Crystallogr., Sect. A: Found. Adv.* **2015**, *71*, 3−8.
(20) Sheldrick, G. M. A short history of SHELX. *Acta Crystallogr., Sect. A: Found. Crystallogr.* **2008**, *64*, 112−122.
(21) Dolomanov, O. V.; Bourhis, L. J.; Gildea, R. J.; Howard, J. A. K.; Puschmann, H. OLEX2: a complete structure solution, refinement and analysis program. *J. Appl. Crystallogr.* **2009**, *42*, 339.
(22) Spek, A. L. Platon Squeeze: a tool for the calculation of the disordered solvent contribution to the calculated structure factors. *Acta Crystallogr., Sect. C: Struct. Chem.* **2015**, *71*, 9−18.
(23) Sheldrick, G. M. Crystal structure refinement with SHELXL. *Acta Crystallogr., Sect. C: Struct. Chem.* **2015**, *71*, 3−8.
(24) Putz, H.; Brandenburg GbR, K.In *Diamond - Crystal and Molecular Structure Visualization, Crystal Impact*; & Bonn, Germany; http://www.crystalimpact.com/diamond.
(25) Boldish, S. I.; White, W. B. Optical Band Gaps of Selected Ternary Sulfide Minerals. *Am. Mineral.* **1998**, *83*, 865−871.
(26) Escobedo-Morales, A.; Ruiz-López, I. I.; Ruiz-Peralta, M. de L.; Tepech-Carrillo, L.; Sánchez-Cantú, M.; Moreno-Orea, J. E. Automated Method for the Determination of the Band Gap Energy of Pure and Mixed Powder Samples Using Diffuse Reflectance Spectroscopy. *Heliyon* **2019**, *5*, e01505.
(27) Michalow, K. A.; Logvinovich, D.; Weidenkaff, A.; Amberg, M.; Fortunato, G.; Heel, A.; Graule, T.; Rekas, M. Synthesis, Characterization and Electronic Structure of Nitrogen-Doped TiO_2 Nanopowder. *Catal. Today* **2009**, *144*, 7−12.
(28) Haushalter, R. C. Synthese und Struktur neuer HgTe-Polyanionen: $[Hg_4Te_{12}]^{4-}$, ein Clusteranion mit Te^{2-}, Te_2^{2-} und Te_3^{2-}, sowie $[Hg_2Te_5]^{2-}$, ein neues Eindimensionales Anorganisches Polymer. *Angew. Chem.* **1985**, *97*, 414−415.
(29) Yang, L.; Powell, D. R.; Houser, R. P. Structural Variation in Copper(I) Complexes with Pyridylmethylamide Ligands: Structural Analysis with a New Four-Coordinate Geometry Index, T4. *Dalton Trans.* **2007**, *9*, 955−964.
(30) Kim, K. W.; Kanatzidis, M. G. Synthesis, Structure and Properties of the Polychalcogenides $[M_4Te_{12}]^{4-}$ (M = Cd, Hg). *Inorg. Chim. Acta* **1994**, *224*, 163−169.
(31) Almond, M. J.; Yates, C. A.; Rice, D. A.; Hendra, P. J.; Brain, P. T. Vibrational Spectroscopy of Dimethyl Telluride, Diethyl Telluride and Di-Tert-Butyl Telluride in the Liquid Phase. *J. Mol. Struct.* **1990**, *239*, 69−82.